BIOCHEMISTRY
including biophysical chemistry & molecular biology

Article

pubs.acs.org/biochemistry

Protonation States of Important Acidic Residues in the Central Ca^{2+} Ion Binding Sites of the Ca^{2+}-ATPase: A Molecular Modeling Study

Maria Musgaard,[†,‡] Lea Thøgersen,[‡,§] and Birgit Schiøtt*[,†,∥]

[†]Department of Chemistry, Aarhus University, Langelandsgade 140, DK-8000 Aarhus C, Denmark

[‡]Centre for Membrane Pumps in Cells and Disease (PUMPKIN), Department of Molecular Biology, Aarhus University, Gustav Wieds Vej 10C, DK-8000 Aarhus C, Denmark

[§]Bioinformatics Research Centre, Aarhus University, C. F. Møllers Allé 8, DK-8000 Aarhus C, Denmark

[∥]Center for Insoluble Protein Structures (inSPIN) and Interdisciplinary Nanoscience Center (iNANO), Department of Chemistry, Aarhus University, DK-8000 Aarhus C, Denmark

Supporting Information

ABSTRACT: The P-type ATPases are responsible for the transport of cations across cell membranes. The sarco(endo)-plasmic reticulum Ca^{2+}-ATPase (SERCA) transports two Ca^{2+} ions from the cytoplasm to the lumen of the sarco(endo)-plasmic reticulum and countertransports two or three protons per catalytic cycle. Two binding sites for Ca^{2+} ions have been located via protein crystallography, including four acidic amino acid residues that are essential to the ion coordination. In this study, we present molecular dynamics (MD) simulations examining the protonation states of these amino acid residues in a Ca^{2+}-free conformation of SERCA. Such knowledge will be important for an improved understanding of atomistic details of the transport mechanism of protons and Ca^{2+} ions. Eight combinations of the protonation of four central acidic residues, Glu309, Glu771, Asp800, and Glu908, are tested from 10 ns MD simulations with respect to protein stability and ability to maintain a structure similar to the crystal structure. The trajectories for the most prospective combinations of protonation states were elongated to 50 ns and subjected to more detailed analysis, including prediction of pK_a values of the four acidic residues over the trajectories. From the simulations we find that the combination leaving only Asp800 as charged is most likely. The results are compared to available experimental data and explain the observed destabilization upon full deprotonation, resulting in the entry of cytoplasmic K^+ ions into the Ca^{2+} binding sites during the simulation in which Ca^{2+} ions are absent. Furthermore, a hypothesis for the exchange of protons from the central binding cavity is proposed.

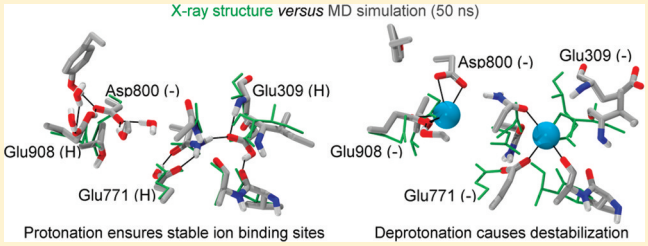

Proteins that belong to the superfamily of P-type ATPases are found in both prokaryotes and eukaryotes, and these essential proteins translocate cations such as H^+, K^+, Na^+, and Ca^{2+} across biological cell membranes by primary active transport.[1] The structurally best characterized P-type ATPase is the sarco(endo)plasmic reticulum Ca^{2+}-ATPase (SERCA) with more than 30 high-resolution crystal structures available (e.g., refs 2−5), including structures of several different conformational states of the catalytic cycle. SERCA is responsible for terminating muscle contractions by transporting Ca^{2+} ions from the cytoplasm and into the lumen of the sarcoplasmic reticulum (SR) where Ca^{2+} ions are stored. The energy for the transport is obtained through hydrolysis of ATP, and during the functional cycle, the protein thus becomes phosphorylated and dephosphorylated, hence the name "P-type".[6] The phosphorylation of the protein by the γ-phosphate of ATP is coupled to large-scale conformational changes driving the transport of Ca^{2+} ions as recently reviewed in detail by Møller et al.[7]

During a single functional cycle, hydrolyzing one ATP molecule, two Ca^{2+} ions are transported from the cytoplasm to the lumen of the SR.[8] In addition to the transport of Ca^{2+} ions, SERCA countertransports protons.[9] For each functional cycle, two or three protons, depending on the pH, are transported from the SR lumen to the cytoplasm.[9−12] The countertransport of two protons is most likely, while the countertransport of four protons can be completely dismissed because that scenario would not give rise to the measured electrostatic currents.[12]

The overall conformation of SERCA is described by either E1 (Ca^{2+}-bound form) or E2 (Ca^{2+}-free, protonated form), similar to what was first proposed for the Na^+/K^+-ATPase.[13,14] In the E1 state, the cation binding sites face the cytoplasm, the Ca^{2+} affinity is high, and the protein works as a kinase phosphorylating Asp351. In the E2 state, the cation binding sites face the SR lumen, the Ca^{2+} affinity is low, and the protein works as a phosphatase. For the sake of simplicity, we will here

Received: July 28, 2011
Revised: November 7, 2011
Published: November 14, 2011

ACS Publications © 2011 American Chemical Society

refer to these forms mainly as a Ca^{2+}-bound form (i.e., E1) and Ca^{2+}-free form (i.e., E2).

The structure of SERCA is comprised of a transmembrane (TM) domain consisting of 10 TM helices, termed TM1−10, and a cytoplasmic headpiece as illustrated in Figure 1A. The

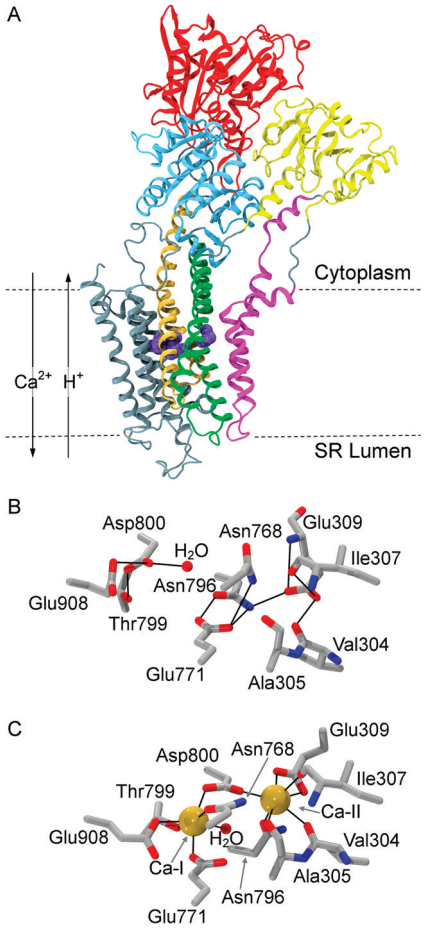

Figure 1. Structure of SERCA and the Ca^{2+} ion binding sites. (A) Structure of SERCA in a conformation deprived of Ca^{2+} ions and ATP (PDB entry 3NAL, resolution of 2.65 Å[24]). The N-domain is colored red, the A-domain yellow, and the P-domain blue; TM1 and TM2 are colored magenta, TM3 and TM4 green, TM5 and TM6 ochre, and TM7−TM10 and loop regions gray. Glu309, Glu771, Asp800, and Glu908 in the middle of the TM domain are involved in Ca^{2+} ion coordination in the Ca^{2+}-bound state and are shown in violet vdW representation to indicate the position of the Ca^{2+} ion binding sites. The approximate position of the membrane is indicated, and the directions of transport of Ca^{2+} ions and protons are noted. (B) Enlargement of the unoccupied Ca^{2+} ion binding sites showing the residues that coordinate Ca^{2+} ions in the Ca^{2+}-bound state. Distances of <3.5 Å are marked by black lines. Same structure as in panel A. (C) Enlargement of the Ca^{2+} ion binding sites in the Ca^{2+}-bound state (PDB entry 1T5S, resolution of 2.60 Å[4]). Ca^{2+} ion coordinations are marked by black lines. For panels B and C, backbone atoms of the residues are shown only where relevant, and the same view is used.

Ca^{2+} ion binding sites are located approximately in the middle of the TM domain and are rich in negative charge and oxygen atoms as seen in Figure 1B. When bound, the Ca^{2+} ions are coordinated by four acidic residues (Glu309, Glu771, Asp800, and Glu908) and, additionally, five carbonyl oxygen atoms from either the protein backbone (Val304, Ala305, and Ile307) or from two asparagine side chains (Asn768 and Asn796). In addition to this, the oxygen atoms from the hydroxyl group of Thr799 and a water molecule are found in the binding site (see Figure 1C). The residues framing the binding sites are positioned in TM4−TM6 and TM8. In the Ca^{2+}-bound form of SERCA, the two bound Ca^{2+} ions, separated by 5.7 Å, are termed Ca-I and Ca-II, respectively, with Ca-II located closest to the cytoplasmic side (Figure 1C). The binding sites are likewise termed site I and site II. The cytoplasmic headpiece is composed of three well-defined domains, the P-domain, the N-domain, and the A-domain[2] (see Figure 1A).

The function of SERCA is to transport Ca^{2+} ions from the cytoplasm to the SR lumen and protons in the opposite direction. The countertransport of protons is, however, believed neither to provide energy for transporting Ca^{2+} ions against the concentration gradient nor to cost energy because the SR membrane is known to be permeable to protons.[15] Instead, the protons are believed to be present to neutralize some of the excess negative charge in the unoccupied Ca^{2+} ion binding sites, and time-resolved Fourier transform infrared difference spectroscopy (FTIR) has indicated that at least two carboxyl groups become protonated when Ca^{2+} ions are released from the Ca^{2+}-bound state.[16] These carboxyl groups most likely belong to the residues also involved in high-affinity Ca^{2+} binding.[16] Additionally, from measurements of charge movements across the membrane, it was demonstrated that the pK_a values of some acidic residues, presumably in the Ca^{2+} ion binding sites, increase as the enzyme undergoes the conformational change from the E1P (phosphorylated and Ca^{2+}-bound) to the E2P (phosphorylated and Ca^{2+}-free) state[12] in the catalytic cycle. Furthermore, studying digestion patterns of SERCA at different pH values led Inesi et al.[17] to propose that the conformation of SERCA will change from E2 to E1 when the protons dissociate from the acidic residues due to a destabilization of the E2 state. Thus, the countertransported protons are expected to be bound to some of the four acidic residues in the Ca^{2+} ion binding sites, namely, Glu309, Glu771, Asp800, and/or Glu908, for the purpose of stabilizing the Ca^{2+}-free state. Because the hydrogen atoms are not visible from the X-ray structure, it is not known which of the residues should be protonated in the Ca^{2+}-free state.

Several studies have focused on the countertransport process and the acidic residues that are involved, mostly by computational approaches,[18−20] but also mutational studies and IR experiments have contributed with knowledge leading to suggestions about protonation states.[17,20,21] Continuum electrostatics calculations used for pK_a prediction have suggested that in the Ca^{2+}-free state, Glu771, Asp800, Glu309, and Glu908 (in descending order of probability) should be protonated.[18] Using a similar method, it was, however, additionally argued that Glu908 and Glu58 (outside of the Ca^{2+} ion binding sites) should be protonated in the Ca^{2+}-bound state.[19] On the other hand, studies using multiconformational continuum electrostatics (MCCE) calculations have suggested that both Glu58 and all four Ca^{2+} ion-coordinating acidic residues should be deprotonated in the Ca^{2+}-bound state.[20] In combination with FTIR, such MCCE calculations have further proposed that Glu771, Asp800, and Glu908 are protonated in the Ca^{2+}-free state.[20,21] From those results, Glu309 is not expected to be protonated. However, from protease digestion studies of two mutant proteins, Glu309Gln and Glu771Gln, it was proposed that the Glu309 and Glu771 side chains are protonated in the Ca^{2+}-free state.[17] Overall, the questions of which and how many of the four acidic residues in the

dx.doi.org/10.1021/bi201164b | *Biochemistry* 2011, 50, 11109−11120

unoccupied Ca^{2+} ion binding sites to protonate have still not been answered. Except for molecular dynamics (MD) simulations on the Ca^{2+}-bound state,[19,22] no MD simulation studies have been published comparing the effect of different protonation schemes in the Ca^{2+} ion binding sites of SERCA. A very recent study of the related Na^+/K^+-ATPase studied the protonation of the central ion binding sites in the K^+-loaded E2 state for describing the different cation selectivities exerted in the different functional states.[23] It was found likely that Glu334, Glu786, and Asp815 must be protonated in the so-called E2·P_i state of Na^+/K^+-ATPase, corresponding to Glu309, Glu771, and Glu908 of SERCA, respectively.

In this study, we present comprehensive investigations of this question via MD simulations of the Ca^{2+}-free state using different combinations of protonation states in the unoccupied Ca^{2+} ion binding sites. Furthermore, we explore the effect of deprotonating all of the four acidic residues being studied to determine whether "full" deprotonation destabilizes the Ca^{2+}-free state, as suggested by Inesi et al.,[17] eventually transforming SERCA to be more E1-like. Such a large conformational change is, however, beyond the reach of the 50 ns time scale of this study.

EXPERIMENTAL PROCEDURES

Protonation of the Four Acidic Residues in the Ca^{2+} Ion Binding Sites. A recently determined Ca^{2+}-free SERCA structure with a single thapsigargin-like inhibitor bound[24] was used for the studies presented here. Structures of a Ca^{2+}-free state (E2·P_i-like) with AlF_4^- bound as a transition state analogue for the dephosphorylation reaction have demonstrated that the structural effects of the binding of a thapsigargin-like inhibitor are minimal;[2−5] thus, the same is presumed to be the case for the Ca^{2+}-free E2 state. Based on a visual analysis of the unoccupied Ca^{2+} ion binding sites identifying possible hydrogen bonds, and predictions of the pK_a values by PROPKA 2.0[25,26] for the four acidic residues, the eight protonation schemes shown in Table 1 were chosen for analysis.

Table 1. MD Simulation Setups[a]

setup	Glu309	Glu771	Asp800	Glu908	simulation time (ns)
A	H	H	–	H	50
B	H	H	–	–	10
C	–	H	–	H	10
D	H	H	H	H	50
E	–	–	–	–	50
F	H	H	H	–	50
G	H	–	–	H	10
H	–	H	H	H	10

[a]Different setups used for MD simulations performed to study the protonation states of the unoccupied Ca^{2+} binding sites in the E2 state. "H" denotes that the residue is protonated, and a dash denotes that the residue is treated as negatively charged.

MD Simulation Protocol. The protein structure used as starting structure was a Ca^{2+}-free conformation of SERCA (PDB entry 3NAL[24]) refined in the high-symmetry space group $P4_12_12$ to a resolution of 2.65 Å. The structure was obtained from crystallization at a close-to-physiological pH value of 6.8 in a mixture of lipid molecules and octaethylene glycol dodecyl ether. We have recently shown that the presence of detergent molecules does not influence the protein structure significantly.[27] Further, the presence of the thapsigargin-like inhibitor is not expected to affect the protein structure as mentioned above. Thus, the crystal structure is expected to represent the physiological protonated E2 functional state well. An alternative structure would be PDB entry 2AGV,[18] refined to a resolution of 2.40 Å but in the lower-symmetry space group $P4_1$. Furthermore, this structure binds an additional inhibitor (2,5-di-*tert*-butylbenzene-1,4-diol), which could impose structural changes on potential ion binding pathways.

The bound thapsigargin analogue was deleted from the protein together with a Mg^{2+} ion. The Mg^{2+} ion is coordinated by both an ATP molecule and the protein in ATP-bound states;[4] however, the ion has not been shown to be important for the ATP-free state. The protein, a structurally bound K^+ ion,[28] and the crystallographically resolved water molecules were retained. A disulfide bond was incorporated between Cys876 and Cys888,[29] and protonation states for the four acidic residues in the vacant Ca^{2+} ion binding sites were chosen as noted in Table 1 for the eight setups. Other protonation states were assigned using the PROPKA-predicted pK_a values and visual analysis. Asp703, with a predicted pK_a value of 8.9 and located close to Asp351 and Asp707 in the P-domain, was protonated as suggested by PROPKA 2.0. The different setups are summarized in Table 1.

The protein was embedded in a 115 Å × 125 Å palmitoyloleoylphosphatidylcholine (POPC) membrane generated by the membrane builder of VMD.[30] SERCA is in vivo positioned in the SR membrane. POPC has been described as a reasonable model for the native SR membrane;[27] thus, a POPC membrane was chosen for the MD studies. The protein was positioned in the membrane as suggested by the Orientation of Proteins in Membrane database.[31] The system was solvated using the Solvate package of VMD, employing the TIP3P water model,[32] to produce a simulation box with dimensions of 115 Å × 125 Å × 163 Å. KCl was added to neutralize and to give an ionic concentration of 0.2 M with the VMD Ionize plugin. Final systems had a size of around 204000 atoms.

MD simulations were performed utilizing NAMD version 2.6[33] and applying the CHARMM27 force field,[34] including the CMAP correction for the protein backbone dihedral angles.[35] The parameters for counterions, K^+ and Cl^-, from Beglovd and Roux[36] were employed as included in the CHARMM27 force field. The potential energy for each system was initially minimized for 15000 steps followed by an equilibration of the lipid tails, in which the tails of the lipids were free to move while the rest of the system was fixed. The lipid equilibration was performed in the NVT ensemble for 0.5 ns. A temperature of 310 K was maintained by applying Langevin dynamics with a damping coefficient of 0.1 ps^{-1}. Following lipid equilibration, the system was released and every atom was free to move in the NPT ensemble for 2 ns. The damping coefficient for controlling the temperature (310 K) with Langevin dynamics was 0.5 ps^{-1}. A pressure of 1 atm was maintained using the Langevin piston Nosé-Hoover method[37,38] with a piston period of 100 fs and a damping time scale of 50 fs.

To control the fluidity of the membrane, the area of the membrane was fixed after 2 ns, changing to the NP_ZAT ensemble for the remaining simulation time. Temperature and pressure were controlled as for the NPT ensemble. Periodic boundary conditions were adopted, and the particle mesh Ewald method[39]accounted for electrostatics with a maximal grid spacing of 1 Å. A cutoff of 12 Å was used for short-range

nonbonded interactions with a switching function starting at 10 Å. The pair list with a cutoff of 14 Å was updated every 20 steps. A time step of 1 fs was used for evaluating all bonded interactions, while short-range nonbonded interactions were evaluated every 2 fs and full electrostatics every 4 fs. Snapshots were written every picosecond. The total simulation times for each system are listed in Table 1. For the purpose of checking the reproducibility of the results, the simulation with setup A was repeated with exactly the same settings as applied here.

Analysis of MD Simulations. For the analysis of the hydrogen bonding patterns in the vacant Ca^{2+} ion binding sites, all possible hydrogen bonds involving the carboxyl and carboxylate groups of the four acidic residues in the Ca^{2+} ion binding sites were identified for all simulations, employing the Hydrogen Bonds plugin for VMD. For each of these identified hydrogen bonds, the relevant distance between the hydrogen bond acceptor atom and the hydrogen atom (A···H) and the hydrogen bond angle (A···H−D) were measured for all simulations employing every 10th snapshot. The population of each hydrogen bond was calculated as the fraction of the time it was present for each simulation using a distance cutoff of 2.5 Å for the A···H distance and a cutoff of 120° for the A···H−D angle. Hydrogen bonds present for at least 10% of the simulation time for at least one simulation were considered in the analysis of the hydrogen bonding pattern.

Prediction of pK_a values as a function of time was performed with a locally installed version of PROPKA 3.0.[40] PROPKA predicts the pK_a values by calculating environmental perturbations of pK_a values and adds these to the intrinsic pK_a value.[25,26,40] Snapshots of the protein structure extracted from the simulation every nanosecond were used for the pK_a prediction.

RESULTS

In this paragraph, the relevance of the chosen protonation setups is outlined before we move to a presentation of the results from the MD simulations. An initial visual analysis of the Ca^{2+} ion binding sites suggests that Glu309, Glu771, and at least one of the residues Asp800 or Glu908 are protonated. This suggestion follows from identifying heteroatom distances of <3.5 Å as indicated in Figure 1B. On this basis, Glu309 must be protonated because of the proximity of backbone carbonyl oxygen atoms of Val304 and Ile307 to the carboxylate group of Glu309. Glu771 is probably protonated because of the short distance between the carboxylate and Asn796(Oδ). Furthermore, the carboxylate groups of Asp800 and Glu908 are located close to one another, and therefore, at least one of these is expected to be neutral. Both of these scenarios were tested in setups A and F, respectively (see Table 1). In setup B, a proton is removed from Glu908 to test whether a proton was really required on either Asp800 or Glu908 to retain binding site stability. The pK_a values of the four acidic residues, Glu309 (pK_a = 6.5), Glu771 (pK_a = 8.0), Asp800 (pK_a = 5.2), and Glu908 (pK_a = 12.2), were further predicted by PROPKA 2.0[25,26] and used for assignment of protonation states. At a physiological pH of approximately 7.4, the predicted pK_a value for Glu908 therefore suggests it to be fully protonated, Asp800 does not seem to be protonated, and Glu771 is suggested to be predominantly protonated. In contrast to the visual inspection, Glu309 should only be protonated to a small extent on the basis of the predicted pK_a value, assuming that the pH inside the protein is comparable to the exterior physiological pH. Such a protonation scheme is tested as setup C. In setup D, a proton on Asp800 was added compared to setup A to investigate if both Asp800 and Glu908 might be protonated, as suggested by other studies.[17,20,21] In setup E, all protons were removed from the four acidic residues being studied to examine whether full deprotonation results in destabilization of the Ca^{2+}-free state in a manner similar to the proposal of Inesi et al.[17] Setup G was run to inspect how the stability was affected by deprotonation of Glu771. Finally, setup H tested the protonation scheme suggested by a combination of time-resolved FTIR and MCCE calculations.[20,21]

The analysis of the MD simulations focused on protein stability, the hydrogen bonding patterns in the unoccupied Ca^{2+} ion binding sites, and visual inspections of the organization of the residues in these binding sites. The aim was to identify a protonation scheme of the acidic Ca^{2+} ion coordinating residues that results in a stable protein structure resembling the crystal structure. First, all setups were studied after simulation for 10 ns. Following this analysis, the most stable and functionally interesting setups were selected and the simulations were continued to 50 ns. Additionally, setup E, with fully deprotonated ion binding sites, was also continued to 50 ns to follow the observed destabilization on a longer time scale. Finally, the 50 ns simulations were analyzed as described for the 10 ns simulations, and furthermore, predictions of pK_a values along these trajectories were undertaken.

Protein Stability. The simulations using setups A−H were analyzed after MD simulation for 10 ns. The stability of the protein was assessed by examining the root-mean-square deviations (rmsd's) for the different setups. The overall rmsd's for the eight different setups relative to the crystal structure are shown in Figure S1 of the Supporting Information. It is found that the rmsd values for all setups fell between 2 and 3.5 Å after simulation for 10 ns. Rmsd values of >5 Å have recently been reported for 10 ns simulations of a Ca^{2+}-bound state of SERCA;[22] thus, the rmsd values reported for setups A−H were well within an acceptable range of a stable SERCA protein. The fluctuations and the size of the rmsd can mainly be ascribed to interdomain movements, and Figure S2 of the Supporting Information shows rmsd graphs for the individual domains for each simulation. It is evident from these graphs that the cytoplasmic domains were in general very stable. Each graph in Figure S2 of the Supporting Information also shows the overall rmsd (including all C_α atoms) and the rmsd for the transmembrane domain. The rmsd of the transmembrane domain was quite stable as well, as discussed below, and thus, the overall higher rmsd's were caused by interdomain movements in the 994-residue large protein. Therefore, the overall protein structure is concluded to be stable in all setups.

Because the acidic residues coordinating the Ca^{2+} ions in the Ca^{2+}-bound state are located in the middle of the transmembrane domain, the effect of altering the protonation states of these residues in the Ca^{2+}-free state would be expected to have a larger impact on the stability of the transmembrane domain than the cytoplasmic domains. The rmsd values for the transmembrane domain seem to fall into two "groups", with setups C, E, and G belonging to one group with slightly higher overall rmsd's and setups A, B, D, F, and H to the other group with overall rmsd's of close to 1 Å (see Figure S1 of the Supporting Information); however, the difference is small.

The root-mean-square fluctuation (rmsf) for the binding site residues (Figure 2) shows that the fluctuation is smallest for setups A, D, and F. For setup B, binding site I with Glu908 fluctuates more, and this is likewise found for site II with

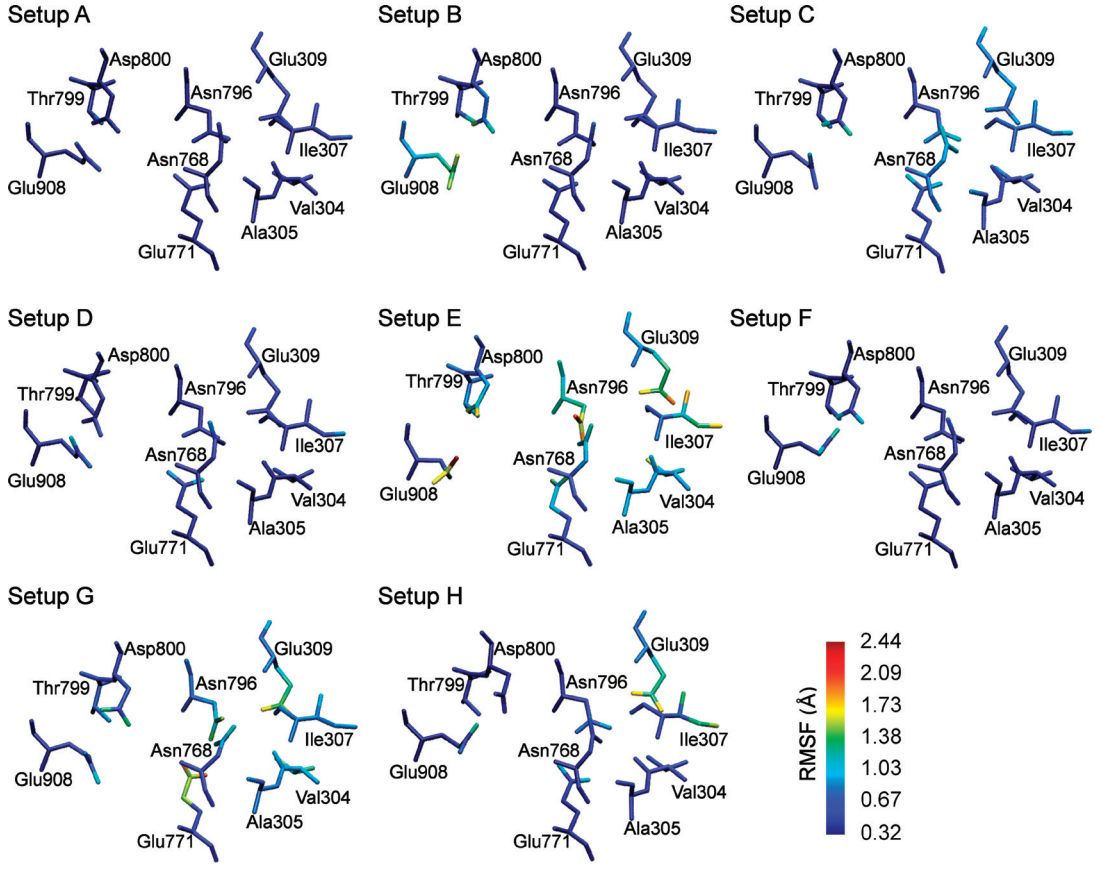

Figure 2. Root-mean-square fluctuations for binding site residues depicted using the color scale shown in the bottom right panel. rmsf values were calculated using 1000 snapshots evenly distributed over the 10 ns trajectory after aligning according to the four helices enclosing the binding sites (TM4–TM6 and TM8).

Glu309 in setup C. For setup E, the fluctuation for all residues, including also backbone regions, is increased. For setup G, especially site II and Glu771 seem to be destabilized, and for setup H, binding site II and Glu309 fluctuate.

Hydrogen Bonding Patterns over 10 ns. A vigorous analysis of possible hydrogen bonding patterns in the unoccupied ion binding sites was undertaken to establish which setups conserve the Ca^{2+} ion binding sites present in the crystal structure the best. The occupancies of the various hydrogen bonds with a carboxyl or carboxylate group of Glu309, Glu771, Asp800, and Glu908 for all eight simulations are summarized graphically in Figure S3 of the Supporting Information. It should be noted that only hydrogen bonds to other protein components and thus not to water molecules were considered. The orientation of the hydrogen bonding residues and the presence of water molecules in the Ca^{2+}-free binding sites after MD simulation for 10 ns were visually analyzed and compared to the crystal structure (see Figure 3). First, it will be outlined why the protonation schemes modeled in setups B, C, E, G, and H result in binding sites where the hydrogen bonding patterns are distorted to such a degree even after 10 ns that the setups can be rejected as irrelevant. Then we continue to show that the protonation schemes modeled in setups A, D, and F result in trajectories conserving the crystal structure environment sufficiently to demand a more thorough investigation.

For setups C, E, and G, which showed the highest rmsd's of the TM domain, the detailed analysis of the hydrogen bonding pattern revealed patterns differing markedly from the pattern expected from the crystal structure. For setup E, the deprotonation of all four acidic residues results in an almost complete lack of the expected hydrogen bonds as evidenced in Figure S3 of the Supporting Information, where especially hydrogen bonds involving Glu309 and Glu771 are absent. This is clearly seen in Figure 3 to lead to a disturbed binding site, and Figure 2 further illustrates considerable fluctuation of the binding site residues. Glu309 is rotated and points the side chain toward a water-filled cavity leading to the cytoplasm (Figure 3). Many water molecules enter the binding site to interact with the four acidic residues, and furthermore, a K^+ ion has entered the site, illustrating that full deprotonation definitely destabilizes the binding site interactions. For setup G, the deprotonated Glu771 is seen in Figure 3 to destabilize the binding site by moving away from Asn796 and instead interacting with many incoming water molecules located in the Glu309 side of the ion binding sites (the Ca-II site). In the Ca-I site, Asp800 does not form any of the expected hydrogen bonds in this setup, as indicated in Figure S3 of the Supporting Information. The deprotonation of Glu309 in setup C disturbs the hydrogen bonding pattern of Glu309, which loses the hydrogen bonds to Val304 and Ile307 and makes a hydrogen bond to Gly310 instead (see Figure S3 of the Supporting Information). Glu309 seems to drag Asn796 along, whereby the direct interaction between Glu771 and Asn796 is eventually lost, only being occupied for ~40% of the sampled structures. Thus, for all three protonation schemes present in setups C, E, and G, the hydrogen bonding patterns around both Glu309 and Glu771 are distorted in such a way that they clearly do not

dx.doi.org/10.1021/bi201164b | *Biochemistry* 2011, 50, 11109–11120

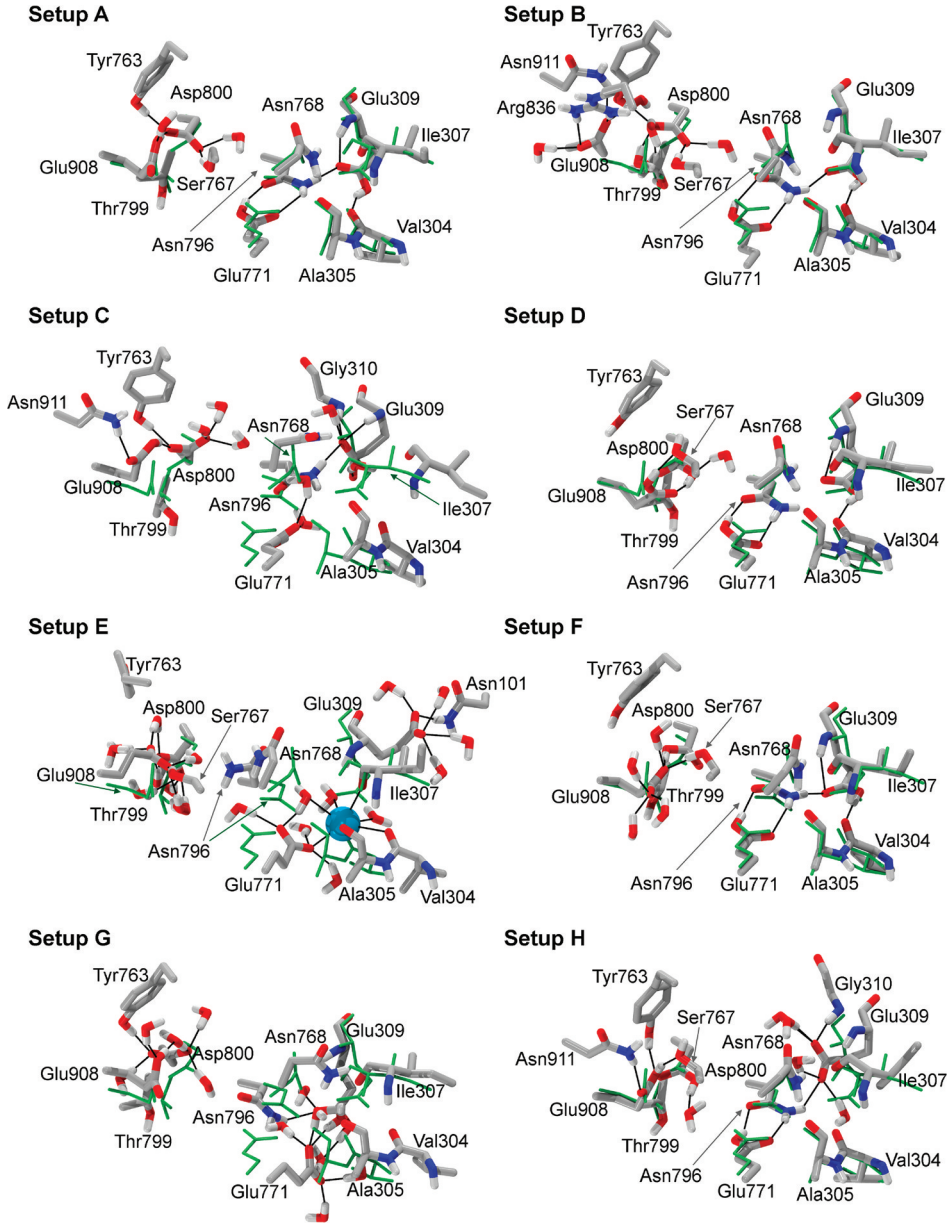

Figure 3. Vacant Ca^{2+} ion binding sites after 10 ns of MD simulation with different amino acid protonation setups (A–H). The position of the Ca^{2+} ion coordinating residues in the crystal structure (PDB entry 3NAL[24]) is included in light green in all panels for comparison. Only water molecules interacting with carboxyl or carboxylate groups of the four acidic residues are included. Hydrogen bond distances involving carboxyl and carboxylate groups with a maximal length of 2.5 Å are shown as black lines. The cyan sphere in panel E shows a K^+ ion that has entered the binding site from the cytoplasm. Ion coordinations are here indicated by black lines. The different snapshots have been superimposed on the crystal structure using membrane-embedded parts of TM4–TM6 and TM8. Only backbone atoms involved in hydrogen bonds with the four acidic residues are shown. Nonpolar hydrogen atoms ahave been omitted.

correspond to the crystal structure. The formation of alternative hydrogen bonding patterns, which seem highly unlikely on the basis of the crystal structure, is observed, e.g., Glu309(Oε)–Gly310(HN) in setup C, Glu309(Hε)–Glu771(Oε) in setup G, and Glu309(Oε)–Asn101(Hδ21) in setup E (see Figure S3 of the Supporting Information).

For setup H, where Glu309 is deprotonated as in setups C and E discarded above, the hydrogen bonding pattern for Glu309 is also unacceptably perturbed and Glu309 interacts with incoming water molecules as visible in Figure 3. From Figure S3 of the Supporting Information, it is seen that the expected interaction with Asn796 is almost fully lost (an occupancy of ~20% is found), and as for setup C, the alternative hydrogen bond to Gly310(HN) is observed. Also, hydrogen bonds to Val304(O) and Ile307(O) are, of course, not possible as no hydrogen bond donor is present. On the Asp800–Glu908 side (Ca-I binding site), where both residues are protonated, the interaction between these residues is lost toward the end of the simulation and is therefore not present in Figure 3, although it is distinctly present in Figure S3 of the Supporting Information.

From the crystal structure, a hydrogen bond between Asp800 and Glu908 is expected. For setups E and B, where both Asp800 and Glu908 are deprotonated, this hydrogen bond is of course not present, whereas it is observed in all other protonation schemes as a well-retained interaction between

dx.doi.org/10.1021/bi201164b | *Biochemistry* 2011, 50, 11109–11120

either Asp800(Hδ) and Glu908(Oε) or Glu908(Hε) and Asp800(Oδ). Instead, Figure S3 of the Supporting Information shows that in setup B, Glu908 forms an interaction with Arg836, which in the crystal structure is located more than 12 Å away, and this results in a destabilization of this part of the binding site as seen in Figure 3. These observations clearly indicate that at least one of the residues Asp800 or Glu908 must be protonated.

From Figures 2 and 3, it is evident that setups A, D, and F have binding site geometries that resemble that of the crystal structure well. All setups have Glu309 protonated, and it is seen from Figure S3 of the Supporting Information that three of the four hydrogen bonds involving Glu309, which are likely to be present in the crystal structure, are maintained in the MD simulations in all three setups. The hydrogen bond between Ile307(O) and Glu309(Hε), which also is expected on the basis of the heteroatom distance in the crystal structure, is not found to be conserved in any of the simulations. However, this hydrogen bond is present as a slightly weaker interaction than expected, as the bond distance and angle fall just outside the acceptance criteria of 2.5 Å and 120°, respectively (see Figure S4 of the Supporting Information). Also, Glu771 is protonated in all these setups and shows well-retained interactions with Asn796(Hδ) and Asn796(Oδ1). For Glu771, two possible hydrogen bonds to the δ-hydrogen atoms of Asn796 has been formed, and therefore, both of these are measured; however, only one of them is expected to be present at a given time. The difference among setups A, D, and F is thus the protonation of Asp800 and Glu908, leaving at most one of them charged. As clearly reflected in Figure S3 of the Supporting Information and described above, this maintains the expected hydrogen bonding between these residues. Overall, this hydrogen bonding pattern analysis shows that to fulfill the goal of reproducing a binding site geometry as observed for the crystal structure, Glu309 should be protonated to retain the side chain in an inward-pointing conformation. Furthermore, Glu771 should be protonated so that the geometry around this residue is not disturbed. Finally, one or two protons are needed on Asp800 and/or Glu908 to keep the binding site stable around these residues. To assess the influence of the protonation states of these two residues further, the simulations with setups A, D, and F were continued to 50 ns. Additionally, setup E, in which all four acidic residues are deprotonated, was similarly continued to 50 ns to study the effect of the deprotonation on a longer time scale, because such a situation has been proposed to result in a more E1-like structure.[17] The full structural transformation is, however, not expected to be observed from a 50 ns MD simulation.

Protein Stability over 50 ns. The overall rmsd's of the four elongated simulations are shown in Figure 4. It is apparent that the rmsd of setup E steadily increases while the overall rmsd's of the other three simulations (setups A, D, and F) level off or increase at a much slower pace. However, setup A has a peak in the overall rmsd after approximately 25 ns. This is caused by a breathing motion between the N-domain and the A-domain, letting them move away from one another with their interdomain distance peaking around 25 ns, and then moving toward each other again. Because the domains are moving toward the initial position after the peak, no overall conformational change is sampled. The rmsd curves of the TM domain alone (Figure 4, bottom panel) reveal that setup E levels off after an initial steep increase over the first couple of nanoseconds; however, it stabilizes at a much higher level than

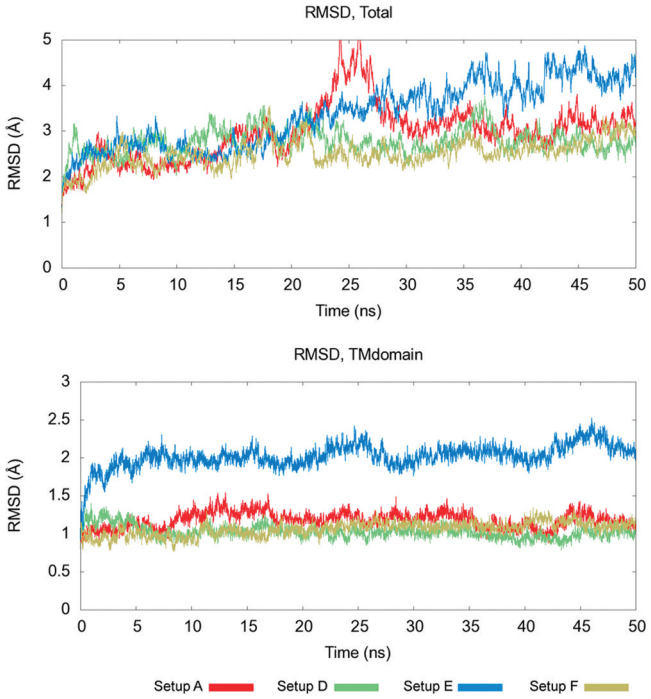

Figure 4. Root-mean-square deviations for MD simulation for 50 ns using setups A and D–F. The top panel shows the rmsd values calculated for all C_α atoms, while the rmsd values in the bottom panel include only C_α atoms in the membrane-embedded domain.

the three other setups. The rmsd values for the individual domains are seen in Figure S5 of the Supporting Information. The rmsd values stabilize at maxima of 2–2.5 Å for the different domains. Thus, full deprotonation of all four acidic residues evidently destabilizes the two ion binding sites, although in an overall stable protein structure in the Ca^{2+}-free state. For setups A, D, and F, no major changes are seen except for the breathing motion in setup A.

Hydrogen Bonding Patterns over 50 ns. The hydrogen bonding patterns for the four acidic residues in the ion binding sites were analyzed as described above, and the data are included in Figure S6 of the Supporting Information. Because setup E has proven to be in a destabilized state on the basis of the analysis of the hydrogen bonding patterns after 10 ns and the entry of a cytoplasmic K^+ ion into the binding sites, as discussed above, this setup is not included in the analysis. Instead, setup E will be treated separately in the Discussion section in relation to functional implications if found. The three-dimensional organization of the binding sites was also studied after 50 ns of MD simulation and is shown in Figure 5.

For all setups, Glu309 is protonated, and no differences are observed in the hydrogen bonding pattern for this residue (Figure S6 of the Supporting Information). Short distances in the crystal structure are reproduced as hydrogen bonds except for that with Ile307; however, as discussed in the analysis of the results after 10 ns, a weak interaction between Glu309 and Ile307 is retained as evident from the distance and angle graphs in Figure S4 of the Supporting Information. Glu771 is also protonated in all setups, resulting in almost similar hydrogen bonding patterns around this residue. The only exception is seen for setup D, in which an unexpected hydrogen bond to Ser767(Hγ) exists for ~50% of the simulation time.

For Asp800 and Glu908, which have different protonation combinations in the three setups, larger differences in the

dx.doi.org/10.1021/bi201164b | *Biochemistry* 2011, 50, 11109–11120

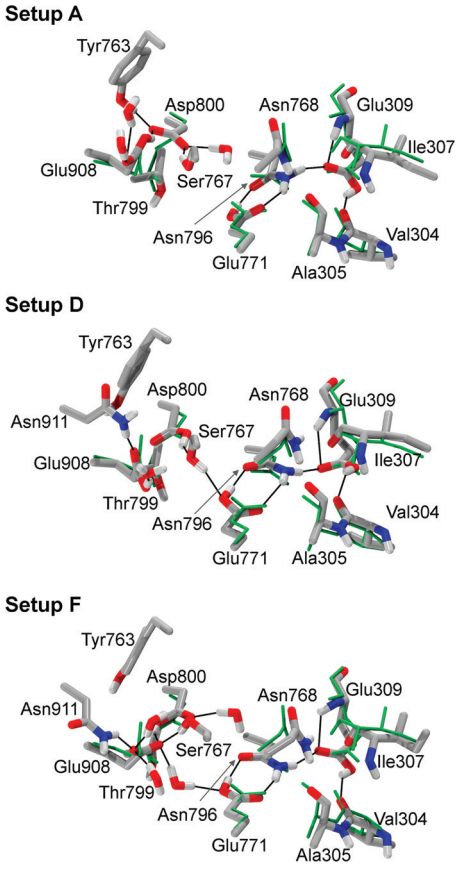

Figure 5. Vacant Ca^{2+} ion binding sites after simulation for 50 ns using setups A, D, and F. Ca^{2+} ion coordinating residues from the crystal structure (PDB entry 3NAL[24]) are included in light green in all panels for comparison. Water molecules interacting with the carboxyl and carboxylate groups of the four acidic residues are included. Hydrogen bond distances involving carboxyl and carboxylate groups with a maximal length of 2.5 Å are shown as black lines. The different snapshots have been superimposed on the crystal structure using membrane-embedded parts of TM4−TM6 and TM8. Nonpolar hydrogen atoms have been omitted.

hydrogen bonding patterns are naturally seen. In setup D, the hydrogen bond between Asp800 and Glu908 is lost after ∼15 ns simulation time, whereby the occupancy for this hydrogen bond is relatively low. Instead, Asp800 makes a hydrogen bond to Ser767, and Glu908 then forms a hydrogen bond to Asn911. In setups A and F, where only either Asp800 or Glu908 is protonated, the hydrogen bond between these residues is conserved throughout the 50 ns simulation time. However, the side chain of Glu908 rotates several times during the simulation of setup F. This causes the hydrogen bond to be shared between the two oxygen atoms of the carboxyl group in Glu908 as evidenced by Figure S6 of the Supporting Information. For both setups A and F, hydrogen bonds not expected on the basis of the crystal structure are additionally formed. For setup A, where Glu908 is protonated, Asp800 interacts with Ser767 and Tyr763, and for setup F, where Asp800 is protonated, Glu908 interacts with Ser767 as illustrated in Figure S6 of the Supporting Information.

In Figure 5, it is seen that all three setups show a binding site resembling the crystal structure very well, the exception being that the Asp800−Glu908 interaction is lost for setup D. It is, however, difficult to judge which protonation combination is most well-suited for describing the protonation in the crystal structure from this analysis. Overall, the hydrogen bonding patterns are relatively stable for the three simulations. The hydrogen bonds which are not predicted from the crystal structure, but observed for setup A, in general have shorter heteroatom distances than the unpredicted hydrogen bonds observed for setups D and F, and furthermore, the Glu908−Asp800 interaction is lost in setup D.

Alteration of Predicted pK_a Values along the Trajectory. To examine whether prediction of pK_a values could disclose which protonation combination of Asp800 and Glu908 is predominant, a snapshot was taken every nanosecond in setups A, D, and F, and pK_a values were predicted for these snapshots. PROPKA-predicted pK_a values for Glu309, Glu771, Asp800, and Glu908 are graphed in Figure 6 as a function of simulation time.

It is seen for Glu309 and Glu771 that predicted pK_a values are quite stable throughout the simulations, and that both of these residues would be expected to be protonated at physiological pH, Glu771 to the largest extent. For setup A, where Asp800 is deprotonated and Glu908 protonated, this is well reproduced in the pK_a prediction for these two residues, where the pK_a value of Asp800 is predicted to be close to 5 and that of Glu908 to be close to 12, much higher than the physiological pH value. On the other hand, both Asp800 and Glu908 are protonated in setup D. This is not reflected in the predicted pK_a values. In the first 15 ns (as long as a hydrogen bond between Asp800 and Glu908 is present), Asp800 is predicted to have a high pK_a and thus to be protonated, while Glu908 is predicted to have a lower pK_a close to 6 and, therefore, to be at least partly deprotonated. After the hydrogen bond between the two residues disappears, Asp800 is predicted to have a pK_a close to the physiological pH, while the predicted pK_a of Glu908 is slightly higher, though fluctuating. Both of the residues only seem to be partly protonated, and in that regard, it seems that there is one proton too many in this setup. For setup F, with Asp800 protonated and Glu908 deprotonated, a scenario opposite to the one seen for setup A would be expected. However, it is seen that the predicted pK_a values are much more fluctuating, with the pK_a of Asp800 sometimes being close to 6 and that for Glu908 sometimes above 11. The fluctuation is clearly coupled between the two residues. It seems as if Asp800 is trying to transfer the proton to Glu908 and Glu908 is ready to accept it; however, this is of course not possible in a force field-based MD simulation.

Overall, on the basis of hydrogen bonding patterns in the binding site and the predicted pK_a values, we find that the protonation scheme used in setup A is the one most likely to be present in the crystal structure of a Ca^{2+}-free functional state of SERCA. On the basis of all the simulations, it is evident that three protons are required in the unoccupied Ca^{2+} ion binding sites to obtain the binding site geometry observed in the crystal structure.[24] Consequently, we find that four protons are not a requirement for obtaining a stable binding site for the Ca^{2+}-free state of SERCA, opposite to what has previously been proposed.[18]

Detailed Analysis of the Glu309 Conformation and pK_a Value. Glu309 has been proposed to be involved in gating the binding of Ca^{2+} ions,[41] and the hydrogen bonding analysis of Glu309 revealed three different positions of the side chain. The simulations propose that when protonated, Glu309 will always be in the most inward-facing conformation seen in setups A, B, D, F, and G. In setup E, with all acidic residues deprotonated, the side chain is observed to flip to an outward-

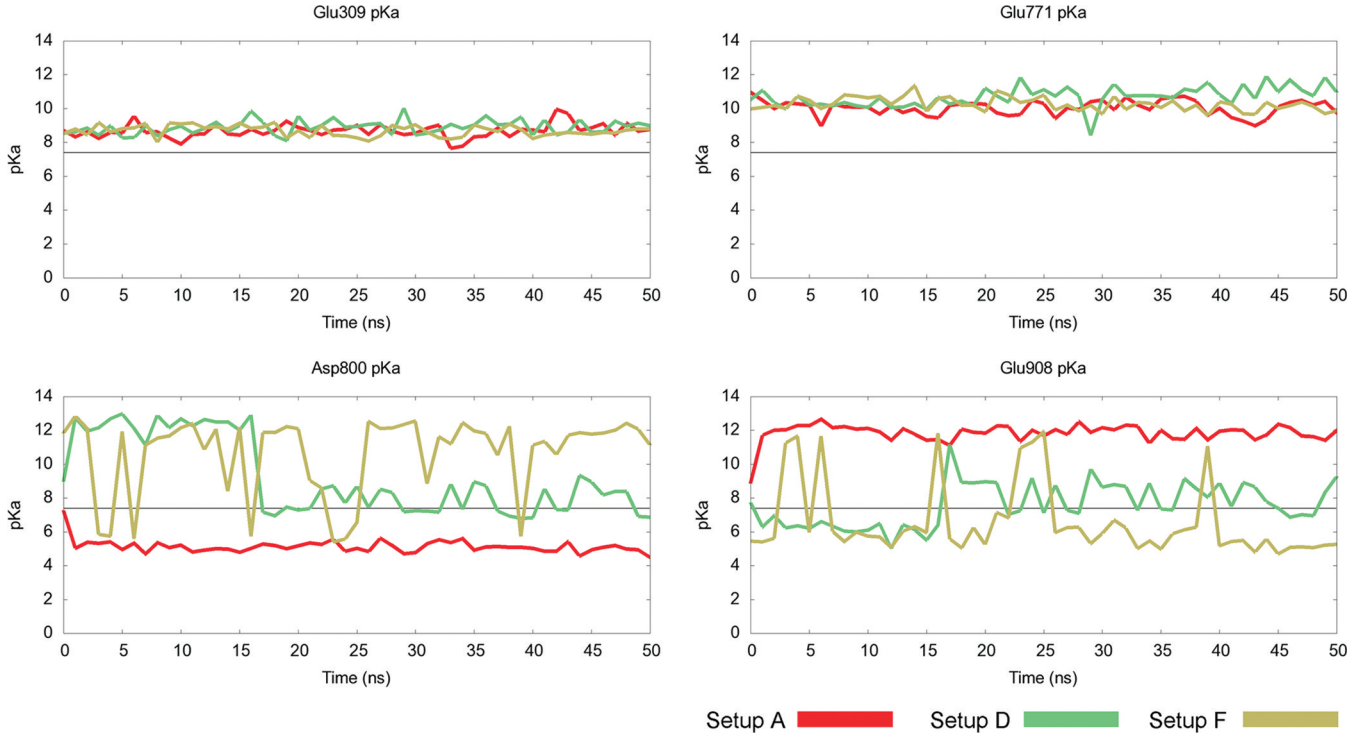

Figure 6. Prediction of pK_a values for the four acidic residues in the unoccupied Ca^{2+} ion binding sites. Predictions were performed with PROPKA 3.0.[40] The black line at pH 7.4 highlights the physiological pH value.

facing conformation (see Figure 3). In setup C, the deprotonated Glu309 has no hydrogen bond to Val304(O) or Ile307(O) as observed in Figure S3 of the Supporting Information; however, the interactions with Glu309(NH) and Asn796(Hδ22) are retained. Additionally, a stable hydrogen bond between the Glu309 side chain and Gly310(NH) is observed. To form the interaction with Gly310, Glu309 has to change its conformation and rotate the side chain, which increases the distance to Val304 and Ile307. Removing the proton on Glu309 and keeping the three other acidic residues protonated in setup H similarly result in a rotation of the side chain of Glu309, forming a hydrogen bond to Gly310(NH) (see Figure S3 of the Supporting Information).

Glu309 has previously[20] been suggested to have two pK_a values and two conformational states, one in which the side chain is pointing toward the other residues in the binding site with a pK_a of ~8.4 and one in which the side chain is pointing out to an apparently water-filled cavity with a pK_a of ~4.7. To evaluate this finding and make connections between the experimental pK_a values and the observed possible conformations of the Glu309 side chain, we predicted pK_a values for Glu309 using PROPKA 3.0[40] for setups A–H from the 10 ns simulations (Figure 7).

From Figure 7, it is seen that the predicted pK_a value for Glu309 is quite stable for the eight simulations, except for setup G where fluctuations are observed, probably caused by the deprotonation of nearby Glu771. If setup G is disregarded, the pK_a is usually predicted to be less than 7.4 when Glu309 is deprotonated (as in setups C, E, and H) and larger than 7.4 if Glu309 is protonated (setups A, B, D, and F). Glu309 is seen to occupy the totally outward-pointing conformation only in setup E, so it seems as if a lower-pK_a conformation pointing more into the binding sites must be found for simulations using setups C and H. It has been suggested from MCCE calculations

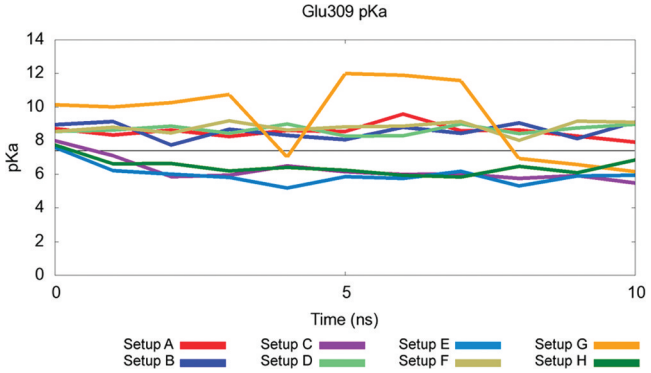

Figure 7. Prediction of pK_a values for Glu309 in the unoccupied Ca^{2+} ion binding site II for the 10 ns simulations. Predictions were performed with PROPKA 3.0.[40] The black line at pH 7.4 highlights the physiological pH value.

that Glu309 resides in both of these conformations (outward and inward, respectively) also when protonated.[20] However, our simulations propose that when protonated, Glu309 resides in the most inward-facing conformation seen in setups A, B, D, and F. No shift to the outward-facing conformation is observed for protonated Glu309, while in setup E, with all acidic residues deprotonated, the side chain is observed to flip to the outward-facing conformation. Notably, for simulations C and H, in which Glu309 is also deprotonated, its side chain is positioned differently, as discussed above (see Figure 3), interacting with Gly310. Other in-house simulations using a Ca^{2+}-free SERCA structure (PDB entry 1XP5[42]), in which Glu309 in the crystal structure is found in the outward-facing conformation, show that when we protonate Glu309 in this conformation and perform an MD simulation, the residue quite quickly flips to a more inward-facing conformation, supporting our finding that

dx.doi.org/10.1021/bi201164b | *Biochemistry* 2011, 50, 11109–11120

this residue is buried when neutral. The results presented here thereby suggest that when protonated, Glu309 always resides in the inward-facing conformation. However, another slightly shifted but still inward-facing conformation is also possible for Glu309, as seen in setups C and H, where the pK_a value is lowered and thus the residue is charged, being depleted of its proton.

DISCUSSION

On the basis of extended MD simulations with eight different combinations of protonation states of the four acidic residues in the Ca^{2+} ion binding sites, we conclude that three bound protons are sufficient to ensure a stable binding pocket, and not four as argued by Obara et al.[18] Rather, protonation of all four residues in our study (setup D) seems to destroy some of the interactions expected on the basis of the crystal structure. As opposed to studies by Hauser and Barth[20] and Andersson et al.,[21] our simulations and pK_a predictions suggest that a proton bound to either Asp800 or Glu908 and not to both is most likely. On the basis of analysis of hydrogen bonding patterns and prediction of pK_a values, Glu908 is more likely to be protonated than Asp800. Possibly, the proton might be able to jump back and forth. Glu309 needs to be protonated to maintain the conformation with an interaction with Val304 and Ile307 as in the crystal structure, and this further requires that Glu771 also be protonated. Either Asp800 or Glu908 should then be protonated as the last residue. Thus, the situation described in setup A seems most likely, where Glu309, Glu771, and Glu908 are all protonated and only Asp800 is charged. To ensure that this result is not a simulation artifact, a repeat of setup A was conducted, giving rise to very similar dynamical properties and hydrogen bonding patterns. Further support for such a protonation scheme in the E2-like states of P-type ATPases may be found in the very recent study by Yu et al.[23] of the E2·P_i state of Na^+/K^+-ATPase. Different simulation methods were used by Yu et al. and ourselves; however, the results for SERCA and the Na^+/K^+-ATPase are very similar in finding that three acidic residues most likely are neutral in E2-like states. The two studies also agree in finding Asp800 (Asp811 in the Na^+/K^+-ATPase) as the ion-binding titratable residue with the lowest pK_a value.

Full deprotonation of all four acidic residues in the Ca^{2+} ion binding sites in the Ca^{2+}-free E2 state has been proposed by Inesi et al.[17] to initiate the transition of the E2 state toward the E1 state because of destabilization. Our simulations indeed confirm that deprotonation destabilizes the interactions in the cation binding sites. Furthermore, it is observed that during the 50 ns simulation, two K^+ ions enter the unoccupied Ca^{2+} ion binding sites from the cytoplasmic side (see Figure 8). For the transition to E1 to occur, Ca^{2+} ions must enter the binding site, so the appearance of other cations in our simulation (Ca^{2+} ions are not included) supports the idea that the observed instability may be en route to an E1 state of SERCA. The entry site and pathway to the binding sites of these cytoplasmic K^+ ions match proposals on Ca^{2+} entry sites and binding pathways recently found in simulations.[43] The question of how the deprotonation of the Ca^{2+}-coordinating residues occurs remains to be answered.

Interestingly, SERCA most likely countertransports two protons[12] as opposed to the three bound protons needed for stability in the Ca^{2+}-free state as demonstrated here. However, even though SERCA is suggested to countertransport two protons, more protons may indeed be bound to the acidic

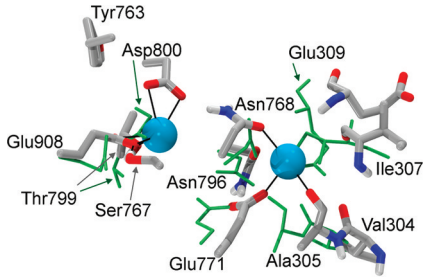

Figure 8. Observed Ca^{2+} ion binding sites after simulation for 50 ns using setup E. Hydrogen bond distances involving carboxylate groups with a maximal length of 2.5 Å are represented as black lines. Ion coordinations are likewise represented as black lines. The cyan spheres are K^+ ions that have entered the binding site from the cytoplasm. Ca^{2+} ion coordinating residues from the starting crystal structure are colored green for comparison. For the sake of clarity, water molecules and nonpolar hydrogen atoms are not shown.

residues in the Ca^{2+}-free form of the protein as protons bound from and released to the same side of the membrane are not registered. In addition, protons have also been suggested to be present in the Ca^{2+}-bound state, attached to Glu908 and Glu58,[19] and that would reduce the number of counter-transported protons compared to the number of protonated residues even more. Others have argued against the binding of protons in the Ca^{2+}-bound state,[20] and our in-house studies on a Ca^{2+}-bound structure (PDB entry 1T5S[4]) suggest that the coordination between Glu908 and the Ca-I ion is lost when Glu908 is protonated (data not shown). The same tendency of Glu908 to loose the direct interaction with Ca-I when it is protonated was reported in a recent MD study by Sugita et al.[22] Therefore, we do not expect that any of the four acidic residues in the Ca^{2+}-bound state are neutral. Still, three protons may very well be present in the Ca^{2+}-free state, while only two become countertransported if one of the protons is bound from and released to the same side of the membrane.

Glu309 has been thought to be an unlikely participant in proton countertransport because it easily can get into contact with the cytoplasm due to the two different identified conformations discussed above.[20] One could imagine that the proton on Glu309 could be bound from the cytoplasmic side, and therefore, it should not be counted as a countertransported proton. Instead, the two protons bound to Glu771 and Glu908 could come from the luminal side and thereby be the countertransported protons. Furthermore, we have seen indications that a low-pK_a inward-facing conformation for Glu309 might exist. This observation is interesting, because Glu309 is believed to gate the access to the ion binding sites.[41] Glu309 would most likely be deprotonated when "delivering" the positively charged Ca^{2+} ions to the binding site. One could speculate that Glu309, in the Ca^{2+}-free form, would be protonated and reside in a higher-pK_a inward-facing conformation. As illustrated in Figure 9 in a schematic way, a small structural change could then move Glu309 to the slightly different inward-facing conformation with a lower pK_a value, where Glu309 would transfer the bound proton to a water molecule and be ready to receive the Ca^{2+} ions and assist them into the binding sites.

These subtle structural changes required would then be expected to be part of the conformational change bringing the Ca^{2+}-free state with occluded binding sites and protonated acidic residues into a slightly more open state where Ca^{2+} ions

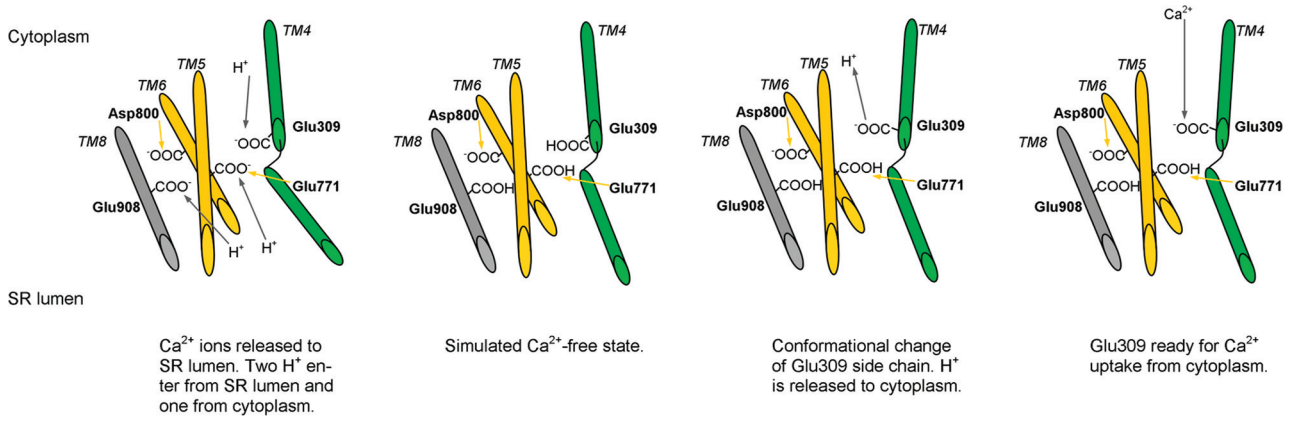

Figure 9. Schematic representation of possible proton exchange in the Ca^{2+}-free state in accordance with the simulation results and experimental observations. The four TM helices contributing to the binding sites are shown as rods in the same color scheme as used for the protein in Figure 1A. The protonation state of the four acidic residues inspected in this study is highlighted.

could bind from the cytoplasmic side. Further studies are in progress in our laboratory to delineate such ideas.

■ ASSOCIATED CONTENT

Supporting Information

Root-mean-square deviation graphs of the individual domains for the 10 ns simulations, hydrogen bonding data, and rmsd graphs relating to the elongated 50 ns simulations. This material is available free of charge via the Internet at http://pubs.acs.org.

■ AUTHOR INFORMATION

Corresponding Author

*E-mail: birgit@chem.au.dk. Fax: +45 8619 6199. Phone: +45 8942 3953.

Funding

This work was supported by the Danish Council for Independent Research | Natural Sciences, the Carlsberg Foundation, the Novo Nordisk Foundation, the Danish Center for Scientific Computing, the Lundbeck Foundation, and the Danish National Research Foundation (inSPIN and PUMPKIN).

■ ACKNOWLEDGMENTS

Prof. Jesper Vuust Møller and Prof. Poul Nissen are thanked for valuable discussions and access to the PDB structure prior to publication.

■ ABBREVIATIONS

FTIR, time-resolved Fourier transform infrared spectroscopy; MCCE, multiconformational continuum electrostatic; MD, molecular dynamics; PDB, Protein Data Bank; POPC, palmitoyloleoylphosphatidylcholine; rmsf, root-mean-square fluctuation; rmsd, root-mean-square deviation; SERCA, sarco-(endo)plasmic reticulum Ca^{2+}-ATPase; SR, sarcoplasmic reticulum; TM, transmembrane.

■ REFERENCES

(1) Møller, J. V., Juul, B., and le Maire, M. (1996) Structural Organization, Ion Transport, and Energy Transduction of P-Type ATPases. *Biochim. Biophys. Acta 1286*, 1−51.

(2) Toyoshima, C., Nakasako, M., Nomura, H., and Ogawa, H. (2000) Crystal Structure of the Calcium Pump of Sarcoplasmic Reticulum at 2.6 Å Resolution. *Nature 405*, 647−655.

(3) Toyoshima, C., and Nomura, H. (2002) Structural Changes in the Calcium Pump Accompanying the Dissociation of Calcium. *Nature 418*, 605−611.

(4) Sørensen, T. L., Møller, J. V., and Nissen, P. (2004) Phosphoryl Transfer and Calcium Ion Occlusion in the Calcium Pump. *Science 304*, 1672−1675.

(5) Olesen, C., Picard, M., Winther, A. L., Gyrup, C., Morth, J. P., Oxvig, C., Møller, J. V., and Nissen, P. (2007) The Structural Basis of Calcium Transport by the Calcium Pump. *Nature 450*, 1036−1042.

(6) Pedersen, P. L., and Carafoli, E. (1987) Ion Motive ATPases. I. Ubiquity, Properties, and Significance to Cell Function. *Trends Biochem. Sci. 12*, 146−150.

(7) Møller, J. V., Olesen, C., Winther, A. L., and Nissen, P. (2010) The Sarcoplasmic Ca^{2+}-ATPase: Design of a Perfect Chemi-Osmotic Pump. *Q. Rev. Biophys. 43*, 501−566.

(8) Inesi, G., Kurzmack, M., Coan, C., and Lewis, D. E. (1980) Cooperative Calcium Binding and ATPase Activation in Sarcoplasmic Reticulum Vesicles. *J. Biol. Chem. 255*, 3025−3031.

(9) Levy, D., Seigneuret, M., Bluzat, A., and Rigaud, J. (1990) Evidence for Proton Countertransport by the Sarcoplasmic Reticulum Ca^{2+}-ATPase during Calcium Transport in Reconstituted Proteoliposomes with Low Ionic Permeability. *J. Biol. Chem. 265*, 19524−19534.

(10) Yu, X., Hao, L., and Inesi, G. (1994) A p*K* Change of Acidic Residues Contributes to Cation Countertransport in the Ca-ATPase of Sarcoplasmic Reticulum. *J. Biol. Chem. 269*, 16656−16661.

(11) Yu, X., Carroll, S., Rigaud, J. L., and Inesi, G. (1993) H^+ Countertransport and Electrogenicity of the Sarcoplasmic Reticulum Ca^{2+} Pump in Reconstituted Proteoliposomes. *Biophys. J. 64*, 1232−1242.

(12) Tadini-Buoninsegni, F., Bartolommei, G., Moncelli, M. R., Guidelli, R., and Inesi, G. (2006) Pre-Steady State Electrogenic Events of Ca^{2+}/H^+ Exchange and Transport by the Ca^{2+}-ATPase. *J. Biol. Chem. 281*, 37720−37727.

(13) Albers, R. W. (1967) Biochemical Aspects of Active Transport. *Annu. Rev. Biochem. 36*, 727−756.

(14) Post, R. L., Hegyvary, C., and Kume, S. (1972) Activation by Adenosine Triphosphate in the Phosphorylation Kinetics of Sodium and Potassium Ion Transport Adenosine Triphosphatase. *J. Biol. Chem. 247*, 6530−6540.

(15) Meissner, G., and Young, R. C. (1980) Proton Permeability of Sarcoplasmic Reticulum Vesicles. *J. Biol. Chem. 255*, 6814−6819.

(16) Barth, A., Kreutz, W., and Mäntele, W. (1997) Ca^{2+} Release from the Phosphorylated and the Unphosphorylated Sarcoplasmic Reticulum Ca^{2+} ATPase Results in Parallel Structural Changes. *J. Biol. Chem. 272*, 25507−25510.

(17) Inesi, G., Lewis, D., Toyoshima, C., Hirata, A., and de Meis, L. (2008) Conformational Fluctuations of the Ca^{2+}-ATPase in the Native Membrane Environment. *J. Biol. Chem. 283*, 1189−1196.

(18) Obara, K., Miyashita, N., Xu, C., Toyoshima, I., Sugita, Y., Inesi, G., and Toyoshima, C. (2005) Structural Role of Countertransport Revealed in Ca^{2+} Pump Crystal Structure in the Absence of Ca^{2+}. *Proc. Natl. Acad. Sci. U.S.A. 102*, 14489−14496.
(19) Sugita, Y., Miyashita, N., Ikeguchi, M., Kidera, A., and Toyoshima, C. (2005) Protonation of the Acidic Residues in the Transmembrane Cation-Binding Sites of the Ca^{2+} Pump. *J. Am. Chem. Soc. 127*, 6150−6151.
(20) Hauser, K., and Barth, A. (2007) Side-Chain Protonation and Mobility in the Sarcoplasmic Reticulum Ca^{2+}-ATPase: Implications for Proton Countertransport and Ca^{2+} Release. *Biophys. J. 93*, 3259−3270.
(21) Andersson, J., Hauser, K., Karjalainen, E., and Barth, A. (2008) Protonation and Hydrogen Bonding of Ca^{2+} Site Residues in the E2P Phosphoenzyme Intermediate of Sarcoplasmic Reticulum Ca^{2+}-ATPase Studied by a Combination of Infrared Spectroscopy and Electrostatic Calculations. *Biophys. J. 94*, 600−611.
(22) Sugita, Y., Ikeguchi, M., and Toyoshima, C. (2010) Relationship between Ca^{2+}-Affinity and Shielding of Bulk Water in the Ca^{2+}-Pump from Molecular Dynamics Simulations. *Proc. Natl. Acad. Sci. U.S.A. 107*, 21465−21469.
(23) Yu, H., Ratheal, I. M., Artigas, P., and Roux, B. (2011) Protonation of Key Acidic Residues is Critical for the K^+-Selectivity of the Na/K Pump. *Nat. Struct. Mol. Biol. 18*, 1159−1163.
(24) Winther, A. L., Liu, H., Sonntag, Y., Olesen, C., le Maire, M., Soehoel, H., Olsen, C., Christensen, S. B., Nissen, P., and Møller, J. V. (2010) Critical Roles of Hydrophobicity and Orientation of Side Chains for Inactivation of Sarcoplasmic Reticulum Ca^{2+}-ATPase with Thapsigargin and Thapsigargin Analogs. *J. Biol. Chem. 285*, 28883−28892.
(25) Li, H., Robertson, A. D., and Jensen, J. H. (2005) Very Fast Empirical Prediction and Rationalization of Protein pK_a Values. *Proteins 61*, 704−721.
(26) Bas, D. C., Rogers, D. M., and Jensen, J. H. (2008) Very Fast Prediction and Rationalization of pK_a Values for Protein-Ligand Complexes. *Proteins 73*, 765−783.
(27) Sonntag, Y., Musgaard, M., Olesen, C., Schiøtt, B., Møller, J. V., Nissen, P., and Thøgersen, L. (2011) Mutual Adaptation of a Membrane Protein and its Lipid Bilayer during Conformational Changes. *Nat. Commun. 2*, 304.
(28) Sørensen, T. L., Clausen, J. D., Jensen, A. L., Vilsen, B., Møller, J. V., Andersen, J. P., and Nissen, P. (2004) Localization of a K^+ Binding Site Involved in Dephosphorylation of the Sarcoplasmic Reticulum Ca^{2+}-ATPase. *J. Biol. Chem. 279*, 46355−46358.
(29) Daiho, T., Yamasaki, K., Saino, T., Kamidochi, M., Satoh, K., Iizuka, H., and Suzuki, H. (2001) Mutations of either or both Cys876 and Cys888 Residues of Sarcoplasmic Reticulum Ca^{2+}-ATPase Result in a Complete Loss of Ca^{2+} Transport Activity without a Loss a Ca^{2+}-Dependent ATPase Activity. *J. Biol. Chem. 276*, 32771−32778.
(30) Humphrey, W., Dalke, A., and Schulten, K. (1996) VMD: Visual Molecular Dynamics. *J. Mol. Graphics 14*, 33−38.
(31) Lomize, M. A., Lomize, A. L., Pogozheva, I. D., and Mosberg, H. I. (2006) OPM: Orientations of Proteins in Membranes Database. *Bioinformatics 22*, 623−625.
(32) Jorgensen, W. L., Chandrasekhar, J., Madura, J. D., Impey, R. W., and Klein, M. L. (1983) Comparison of Simple Potential Functions for Simulating Liquid Water. *J. Chem. Phys. 79*, 926−935.
(33) Phillips, J. C., Braun, R., Wang, W., Gumbart, J., Tajkhorshid, E., Villa, E., Chipot, C., Skeel, R. D., Kalé, L., and Schulten, K. (2005) Scalable Molecular Dynamics with NAMD. *J. Comput. Chem. 26*, 1781−1802.
(34) MacKerell, A. D. Jr., Bashford, D., Bellott, M., Dunbrack, R. L. Jr., Evanseck, J. D., Field, M. J., Fischer, S., Gao, J., Guo, H., Ha, S., Joseph-McCarthy, D., Kuchnir, L., Kuczera, K., Lau, F. T. K., Mattos, C., Michnick, S., Ngo, T., Nguyen, D. T., Prodhom, B., Reiher, W. E. III, Roux, B., Schlenkrich, M., Smith, J. C., Stote, R., Straub, J., Watanabe, M., Wiorkiewicz-Kuczera, J., Yin, D., and Karplus, M. (1998) All-Atom Empirical Potential for Molecular Modeling and Dynamics Studies of Proteins. *J. Phys. Chem. B 102*, 3586−3616.
(35) Mackerell, A. D., Feig, M., and Brooks, C. L. III. (2004) Extending the Treatment of Backbone Energetics in Protein Force Fields: Limitations of Gas-Phase Quantum Mechanics in Reproducing Protein Conformational Distributions in Molecular Dynamics Simulations. *J. Comput. Chem. 25*, 1400−1415.
(36) Beglov, D., and Roux, B. (1994) Finite Representation of an Infinite Bulk System: Solvent Boundary Potential for Computer Simulations. *J. Chem. Phys. 100*, 9050−9063.
(37) Martyna, G. J., Tobias, D. J., and Klein, M. L. (1994) Constant Pressure Molecular Dynamics Algorithms. *J. Chem. Phys. 101*, 4177−4189.
(38) Feller, S. E., Zhang, Y., Pastor, R. W., and Brooks, B. R. (1995) Constant Pressure Molecular Dynamics Simulation: The Langevin Piston Method. *J. Chem. Phys. 103*, 4613−4621.
(39) Darden, T., York, D., and Pedersen, L. (1993) Particle Mesh Ewald: An N·log(N) Method for Ewald Sums in Large Systems. *J. Chem. Phys. 98*, 10089−10092.
(40) Olsson, M. H. M., Søndergaard, C. R., Rostkowski, M., and Jensen, J. H. (2011) PROPKA3: Consistent Treatment of Internal and Surface Residues in Empirical pKa Predictions. *J. Chem. Theory Comput. 7*, 525−537.
(41) Inesi, G., Ma, H., Lewis, D., and Xu, C. (2004) Ca^{2+} Occlusion and Gating Function of Glu^{309} in the ADP-Fluoroaluminate Analog of the Ca^{2+}-ATPase Phosphoenzyme Intermediate. *J. Biol. Chem. 279*, 31629−31637.
(42) Olesen, C., Sørensen, T. L., Nielsen, R. C., Møller, J. V., and Nissen, P. (2004) Dephosphorylation of the Calcium Pump Coupled to Counterion Occlusion. *Science 306*, 2251−2255.
(43) Musgaard, M., Thøgersen, L., Schiøtt, B., and Tajkhorshid, E. Tracing Cytoplasmic Ca^{2+} Ion and Water Access Points in the Ca^{2+}-ATPase. Manuscript submitted to Biophys. J.